WEP Warwick Evans Publishing

International Journal of Mechanical and Electrical Engineering

ISSN: 3005-9615 (Print), ISSN: 3005-7132 (Online)
Volume 8, Number 8, Year 2026
DOI: https://doi.org/10.62051/ijmee.v8n8.07

Dynamic Simulation and Hysteresis Compensation Control of Piezoelectric Actuators Based on Feedforward Inverse P-I Model and PID

Li Liang *

School of Mechanical Engineering, University of Shanghai for Science and Technology, Shanghai, China

* Corresponding Author: Li Liang

ABSTRACT

Piezoelectric actuators are widely used in precision force tracking and active vibration control due to their high stiffness and rapid response. However, the inherent hysteresis nonlinearity severely degrades their tracking accuracy. To address this issue, this paper proposes a hybrid control strategy combining an asymmetric Prandtl-Ishlinskii (P-I) inverse model feedforward with PID feedback. First, the asymmetric P-I forward model is established to describe the non-symmetric hysteresis loop, and its weights are identified using the least-squares method based on normalized experimental data. Subsequently, the P-I inverse model is derived via the geometric method and employed as a feedforward compensator to linearize the actuator. A PID controller is connected in parallel to suppress external disturbances and model mismatch. Finally, the proposed hybrid controller is validated in MATLAB/Simulink under step, sinusoidal, and irregular triangular wave inputs. The simulation results demonstrate that, compared with the conventional pure PID controller, the hybrid control strategy significantly eliminates the hysteresis effect and improves the tracking accuracy. The root-mean-square error (RMSE) is reduced by more than 75% on average, verifying the effectiveness and robustness of the proposed strategy for high-precision force-tracking engineering applications.

KEYWORDS

Piezoelectric Actuator; Hysteresis Compensation; Prandtl-Ishlinskii Model; Feedforward-PID Control.

1. INTRODUCTION

Piezoelectric actuators have been widely applied in micro-robots, scanning tunneling microscopes, and other precision systems due to their fast response, high power density, and high stiffness[1-3]. However, the inherent hysteresis and creep characteristics of piezoelectric materials severely degrade the control accuracy in practical applications, potentially leading to system instability. A comprehensive survey on various control challenges arising from hysteresis nonlinearity in nanopositioning systems can be found in Ref.[4]. Therefore, it is necessary to model the hysteresis nonlinearity and develop high-precision control strategies for piezoelectric actuators.

Regarding the modeling of piezoelectric hysteresis, various methods such as the Preisach model and the Bouc-Wen model have been proposed. Among them, the Prandtl-Ishlinskii (P-I) model has been widely adopted in engineering practice due to its advantages of an analytical inverse, low computational cost, and ease of parameter identification. Nevertheless, the classical P-I model is limited to symmetric hysteresis loops and fails to capture the asymmetric behavior widely observed

Content from this work may be used under the terms of CC BY-NC 4.0 licence (https://creativecommons.org/licenses/by-nc/4.0/).
Published by Warwick Evans Publishing.

in practical piezoelectric actuators[5]. Various improved asymmetric P-I structures have been proposed to address this drawback. The standard P-I model is constructed by a weighted superposition of multiple Play operators, and its parameters can be efficiently identified using the least-squares method. The ordinary least-squares algorithm provides a straightforward analytical solution for weight identification without iterative optimization[6]. More importantly, the inverse P-I model can be directly derived through a geometric or analytical approach. By placing the inverse model as a feedforward compensator in the forward path of the control loop, the hysteretic actuator can be linearized, which lays the foundation for subsequent linear controller design.

Although the inverse model feedforward can eliminate most of the hysteresis nonlinearity, pure feedforward control is inherently an open-loop scheme. It cannot suppress external disturbances or compensate for model mismatch caused by temperature drift and wear. Therefore, the composite architecture combining P-I inverse feedforward and PID feedback becomes a feasible solution to balance nonlinear compensation and disturbance rejection[7]. In this structure, the feedforward loop handles the primary nonlinear compensation, while the PID feedback loop suppresses external disturbances and corrects residual errors.

In this paper, an asymmetric P-I forward model is established, and its weights are identified using the least-squares method based on normalized experimental data. Subsequently, the P-I inverse model is constructed using the geometric method, and a feedforward-PID hybrid control architecture is designed. The tracking performance of the proposed hybrid control strategy is compared with a conventional pure PID controller in MATLAB/Simulink, providing a reference for the high-precision engineering control of piezoelectric actuators.

2. MODELING OF PIEZOELECTRIC ACTUATOR

2.1. Modeling of Piezoelectric Actuator

The hysteresis of the piezoelectric actuator manifests as a multi-valued relationship between output force and applied voltage; the curves during loading (voltage increasing) and unloading (voltage decreasing) do not coincide. This means the actuator exhibits different outputs for the same voltage value depending on the direction of the voltage change. To accurately describe this characteristic, an asymmetric Prandtl-Ishlinskii (P-I) model is established in this paper.

The P-I model is constructed by the weighted superposition of a finite number of Play operators with different thresholds. Let the input voltage be $v(t)$, and the output of the k-th Play operator at time t_i be $F_k(v(t))$, which is defined as:

$$F_k(v(t)) = max\{v(t) - r_k, min\{v(t) + r_k, F_k(v(t_{i-1}))\}\} \tag{1}$$

where r_k is the threshold of the k-th Play operator, satisfying $0 = r_1 < r_2 < \cdots < r_n$.

Since the classical P-I model can only describe symmetric hysteresis loops, the ascending and descending branches are separated and assigned different weights to fit the actual asymmetric hysteresis curves. The expression of the improved asymmetric P-I model is:

$$f(t) = \sum_{k=1}^{n} (p \cdot w_k^{rise} + q \cdot w_k^{fall}) F_k(v(t)) \tag{2}$$

where w_k^{rise} and w_k^{fall} are the weights of the ascending and descending branches, respectively; n is the total number of operators (n=40 in this paper). p and q are direction selection coefficients:

When $v(t) \geq v(t_{i-1})$ (voltage increasing), p=1, q=0;

When $v(t) < v(t_{i-1})$ (voltage decreasing), p=0, q=1.

2.2. Hysteresis Data Acquisition and Normalization

To identify the model parameters, the actual hysteresis characteristics of the piezoelectric actuator were first obtained through experiments. The initial preload applied by the preload bolt was set to 500 N. A triangular wave voltage signal of 0~100 V was input to the piezoelectric actuator through a power amplifier, and the corresponding output force was recorded to obtain the complete hysteresis loop, as shown in Fig. 1.

Segmentation Extraction Results of Piezoelectric Hysteresis Data

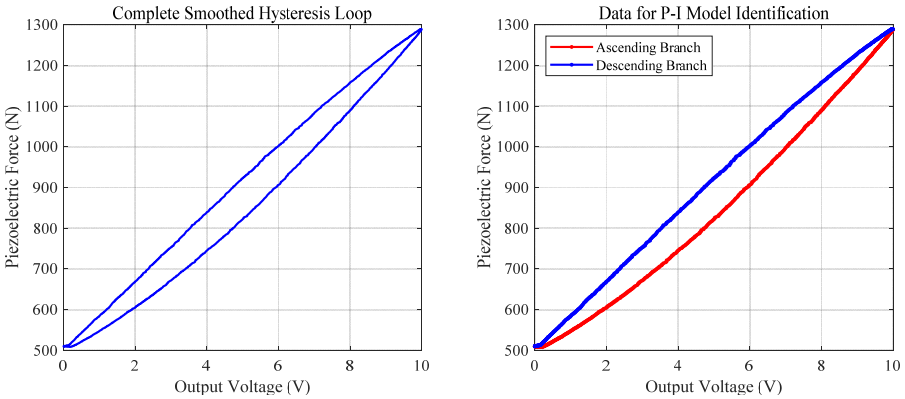


Figure 1. Segmentation Extraction Results of Piezoelectric Hysteresis Data

To eliminate the influence of different dimensions of voltage and force on parameter identification, the experimental data were normalized and mapped to the interval [0,1] before identification:

$$v_n = \frac{v(t) - v(t)_{min}}{v(t)_{max} - v(t)min}, \qquad f_n = \frac{f(t) - f(t)_{min}}{f(t)_{max} - f(t)_{min}} \tag{3}$$

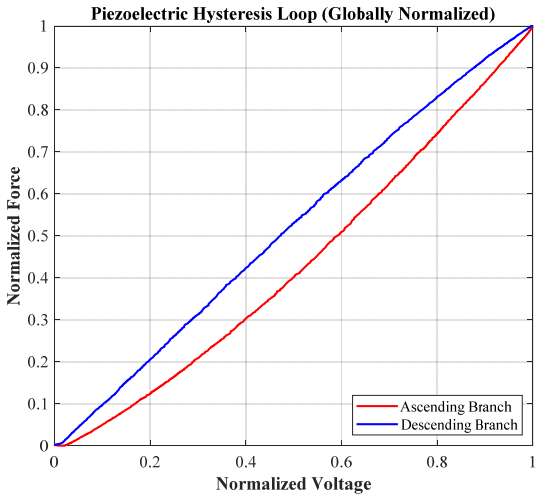


Figure 2. Piezoelectric Hysteresis Loop (Globally Normalized)

2.3. Parameter Identification Based on Least Squares

According to Eq. (2), the output of the P-I model can be written in a linear regression form. For the ascending (or descending) branch, the output can be expressed as:

$$Y = X \cdot W \tag{4}$$

where Y is the column vector of the normalized output force; $W = [w_1, w_2, \ldots, w_n]^T$ is the column vector of weights to be determined; X is the regression matrix of the Play operator outputs, whose element in the i-th row and k-th column is $F_k(v(i))$.

For the collected experimental data, the ordinary least-squares method is used to minimize the residual sum of squares, and its analytical solution is:

$$\mathrm{W} = (X^T\mathrm{X})^{-1}X^T\mathrm{Y} \tag{5}$$

By applying Eq. (5) to the ascending and descending branch data respectively, the weights w_k^{rise} and w_k^{fall} can be obtained through MATLAB programming, as shown in Table 1.

Table 1. Table of thresholds and weights

Threshold_r	Weight_rise_wp	Weight_fall_wq	Threshold_r	Weight_rise_wp	Weight_fall_wq
0	0.04119206	0.75770163	0.5	-0.069673009	0.121118123
0.025	0.57330338	0.079494236	0.525	0.068793616	0
0.05	0.012077527	0.066743482	0.55	0.181533092	0
0.075	0.075580714	0.026046606	0.575	-0.28078484	0
0.1	0.00269323	-0.002656965	0.6	0.273524196	0
0.125	0.02090483	0.044945913	0.625	-0.121474633	0
0.15	0.085427803	0.074327827	0.65	0.034043848	0
0.175	-0.068835013	-0.037282703	0.675	0.00997332	0
0.2	0.057157169	0.00408553	0.7	-0.009043935	0
0.225	0.003826891	0.021895289	0.725	0.092567681	0
0.25	0.057397573	0.045038009	0.75	-0.11264604	0
0.275	0.060828149	-0.012964533	0.775	0.07573817	0
0.3	-0.011333773	-0.014957054	0.8	0.082104497	0
0.325	-0.04147478	0.09232808	0.825	-0.070251677	0
0.35	0.081822077	-0.117383639	0.85	-0.060136794	0
0.375	0.069700028	0.106207834	0.875	0.090123036	0
0.4	-0.132468693	-0.057068604	0.9	0.033095876	0
0.425	0.079639653	-0.011186823	0.925	0.051546756	0
0.45	0.077853207	0.053108367	0.95	-0.070955092	0
0.475	0.0190254	-0.240441537	0.975	0.139666306	0

Substituting the obtained weights into the P-I model and simulating the experimental input data yields the comparison between model output and measured output. The mean-squared-error (MSE) calculated on normalized data is: $\mathrm{MSE}_{rise} \approx 8.0 \times 10^{-7}$, $\mathrm{MSE}_{fall} \approx 2.6 \times 10^{-6}$. The fitting results are shown in Fig. 3.

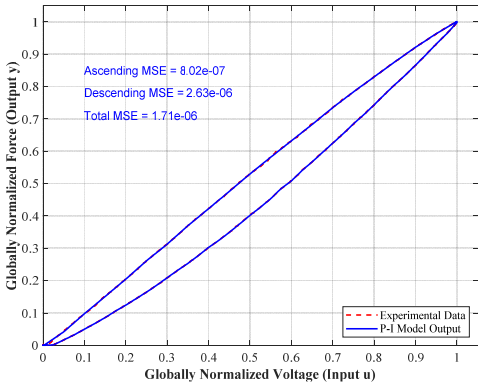


Figure 3. Forward Model Verification

The results indicate that by using the direct least-squares method, the P-I model can describe the hysteresis nonlinearity of the piezoelectric actuator with high precision. Moreover, the separate identification of ascending and descending weights fully reflects the asymmetric hysteresis characteristics.

3. CONTROLLER DESIGN

3.1. P-I Inverse Model

To overcome the phase lag of pure PID control when tracking hysteretic nonlinear objects and the inability of pure feedforward to resist external disturbances, a hybrid feedforward-PID control strategy is designed. To compensate for the hysteresis, a P-I inverse model is established as the feedforward controller.

The inverse model can be obtained using the geometric method: the P-I model and its inverse are symmetric about the line y=v, and the weights and thresholds of the inverse model can be directly derived from the forward model parameters:

$$\begin{cases} w_{p1}^{-1} = \dfrac{1}{w_{p1}} \\ w_{q1}^{-1} = \dfrac{1}{w_{q1}} \\ w_{pk}^{-1} = \dfrac{-W_{pj}}{\left(\sum_{i=1}^{k} w_{pi}\right)\left(\sum_{i=1}^{k-1} w_{pi}\right)} \\ w_{qk}^{-1} = \dfrac{-W_{qj}}{\left(\sum_{i=1}^{k} w_{qi}\right)\left(\sum_{i=1}^{k-1} w_{qi}\right)} \\ r_k^{-1} = \sum_{i=1}^{k} w_{pi}(r_k - r_i) \\ k = 1,2,3,\ldots,n-1,n \end{cases} \tag{6}$$

where w_{pk} and w_{qk} denote the ascending-branch and descending-branch weights of the forward P-I model, respectively. Using Eq. (6), the inverse model weights can be calculated from the forward weights in Table 1, and the inverse fitting verification is shown in Fig. 4.

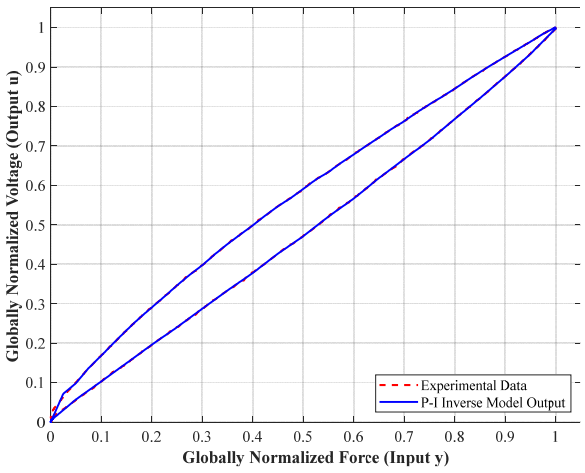


Figure 4. Inverse Model Verification

3.2. Hybrid Feedforward-PID Control Architecture

To balance the dynamic tracking accuracy and anti-disturbance robustness, a hybrid control architecture is designed, as shown in Fig. 5. The system consists of a feedforward channel and a feedback channel in parallel:

1. Feedforward Channel: The desired force signal is input into the inverse P-I model to generate the feedforward voltage command u_{ff}, which counteracts the hysteresis nonlinearity and provides a fast initial response.
2. Feedback Channel: The sensor collects the actual output force and compares it with the desired force to obtain the error $e(t)$. The error signal is input into the PID controller to generate the feedback voltage command u_{fb}, which corrects model errors, suppresses external disturbances, and eliminates steady-state errors.

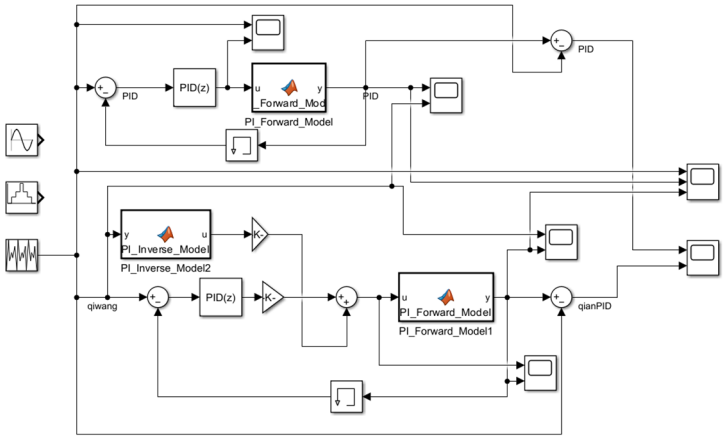


Figure 5. Simulink control block diagram

The total control voltage u(t) is the sum of the feedforward and feedback outputs:

$$u(t) = u_{ff}(t) + u_{fb}(t) \tag{7}$$

The discrete PID controller equation is:

$$u_{fb}(k) = K_p e(k) + K_i \sum_{j=0}^{k} e(j) \triangle t + K_d \frac{e(k) - e(k-1)}{\triangle t} \tag{8}$$

where $\triangle t$ is the sampling period; $e(k) = f_{ref}(k) - f_{act}(k)$; K_p, K_i, and K_d are the proportional, integral, and derivative gains. In this architecture, the feedforward channel undertakes the majority of the nonlinear compensation, significantly reducing the burden on the PID controller.

4. SIMULATION RESULTS AND ANALYSIS

To verify the effectiveness of the proposed feedforward-PID hybrid control strategy, a closed-loop control system simulation model was built in MATLAB/Simulink. In the simulation, the asymmetric P-I forward model identified in Section 2 was used to simulate the real piezoelectric actuator (the controlled plant). The inverse model designed in Section 3 was used as the feedforward controller, connected in parallel with the PID feedback.

To comprehensively evaluate the tracking performance, three different types of reference signals were applied: a step signal, a sinusoidal signal, and an irregular triangular wave signal. The performance of the proposed hybrid controller was compared with a conventional pure PID controller. The simulation step size was set to 1×10^{-5}s. The PID parameters for the pure PID controller were tuned as $K_p = 0.21$, $K_i = 0.2$, $K_d = 0$, while for the hybrid controller, they were set to $K_p = 0.1$, $K_i = 0.1$, $K_d = 0$.

4.1. Tracking Performance Analysis

Fig. 6 presents the comprehensive comparison of tracking trajectories and errors between the pure PID controller and the proposed hybrid controller under the three reference signals.

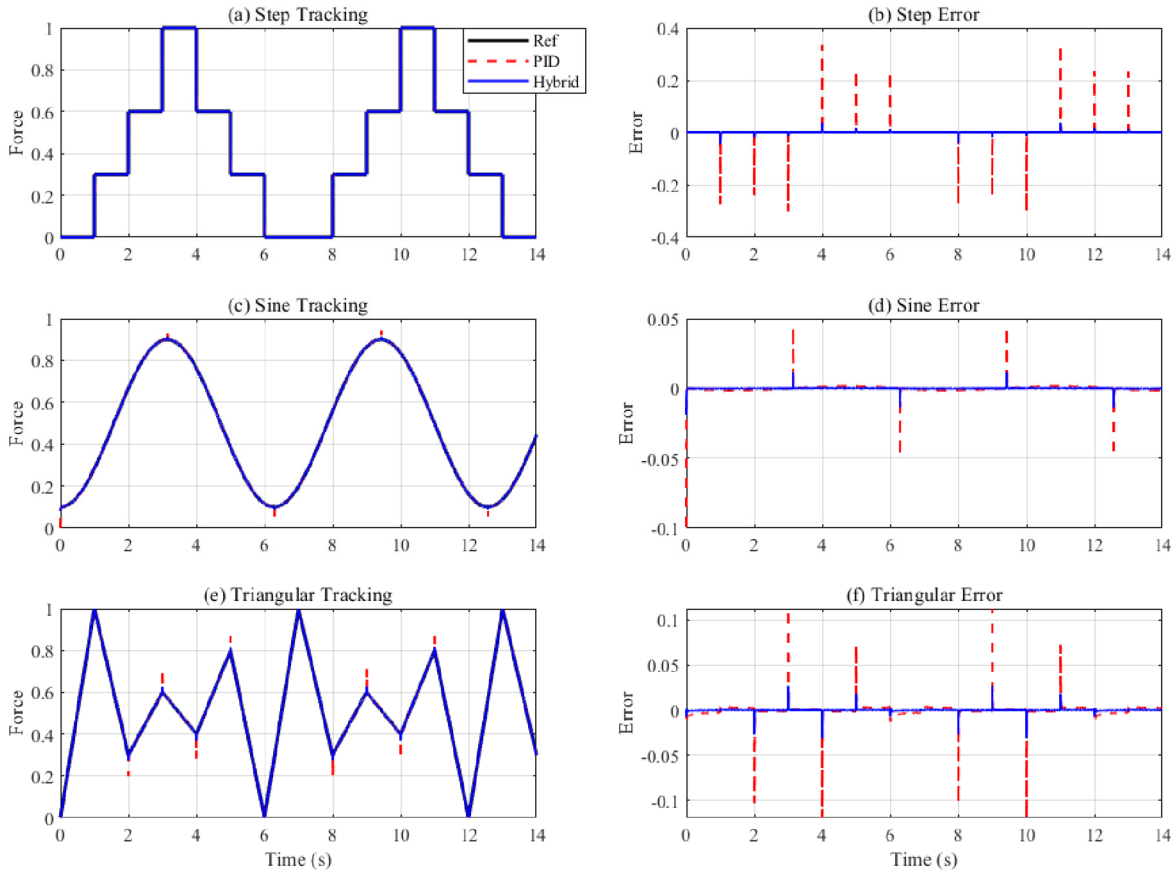


Figure 6. Tracking performance comparison chart

Fig. 6(a) and 6(b) show the transient response under a step reference. Due to the inherent hysteresis, the pure PID controller exhibits significant overshoot and a longer settling time. In contrast, the proposed hybrid controller benefits from the immediate feedforward voltage generated by the inverse model, reaching the target rapidly with almost zero overshoot. The maximum transient error is drastically reduced.

To evaluate dynamic tracking capability, a continuous sinusoidal signal $f_{ref}(t) = 0.5 + 0.4\sin t$ was applied. As shown in Fig. 6(c) and 6(d), the pure PID controller suffers from obvious phase lag and amplitude attenuation, resulting in a large periodic error. The hybrid controller demonstrates excellent performance; the actual trajectory almost perfectly coincides with the reference. The error curve is tightly compressed near the zero line, indicating that the inverse model successfully linearizes the hysteresis.

To test the adaptability to complex, non-smooth signals, an irregular triangular wave with varying slopes was used. As observed in Fig. 6(e) and 6(f), the pure PID struggles at the sharp corners, generating larger transient errors. The hybrid controller handles the sudden reversals effectively. Although minor transient fluctuations occur at the exact turning points (due to the rapid direction switching of the hysteresis weights), the overall tracking error is significantly suppressed compared to the pure PID scheme, proving strong robustness.

4.2. Quantitative Error Analysis

To quantify the tracking performance, the Root Mean Square Error (RMSE) and Maximum Absolute Error ($E_{\max}$) were calculated for the three cases, as summarized in Table 2.

Table 2. Summary Table of Errors

Input_Signal	Emax_PurePID	Emax_Hybrid	Emax_Reduce_Percent	RMSE_PurePID	RMSE_Hybrid	RMSE_Reduce_Percent
Step	0.336207591	0.044841863	86.66%	0.013385777	0.001356418	89.87%
Sine	0.099134967	0.018936456	80.90%	0.002504994	0.000519208	79.27%
Triangular	0.119275809	0.030911086	74.08%	0.005017334	0.001163975	76.80%

The quantitative results indicate that the proposed hybrid controller dramatically reduces both $E_{\max}$ and RMSE across all scenarios. Compared with the pure PID controller, the RMSE of the hybrid control is reduced by over 75% on average. This demonstrates that the composite strategy not only eliminates the hysteresis nonlinearity but also ensures high precision and fast response under various reference inputs.

5. CONCLUSION

In this paper, an asymmetric Prandtl-Ishlinskii (P-I) model and a feedforward-PID hybrid control strategy are proposed to compensate for the hysteresis nonlinearity of piezoelectric actuators. The main conclusions are as follows:

Modeling and Identification: The asymmetric P-I model, constructed by separating the ascending and descending weights, effectively captures the non-symmetric hysteresis behavior. The parameters are identified using the ordinary least-squares method based on normalized experimental data, achieving a high fitting accuracy with an MSE of approximately 8.0×10^{-7} for the ascending branch.

Controller Design: By utilizing the analytical inverse of the P-I model as a feedforward compensator, the hysteretic actuator is successfully linearized. Combined with a PID feedback loop, the hybrid architecture achieves a perfect balance between rapid dynamic response and strong robustness against external disturbances.

Simulation Validation: The proposed strategy is verified under step, sinusoidal, and irregular triangular wave inputs. The simulation results demonstrate that the hybrid controller significantly outperforms the conventional pure PID controller. The Root Mean Square Error (RMSE) and Maximum Absolute Error are reduced by over 75% on average, proving the superiority of the composite control scheme in terms of tracking accuracy and transient stability.

The proposed control framework requires low computational effort and is easy to implement, providing a reliable and practical reference for the high-precision control of piezoelectric actuators in complex engineering applications.

REFERENCES

[1] Uchino, K. (1996). Piezoelectric actuators and ultrasonic motors. Springer Science & Business Media. https://doi.org/10.1007/978-1-4613-1157-1.

[2] Lok, M., Helbling, E. F., Zhang, X., et al. (2017). A low mass power electronics unit to drive piezoelectric actuators for flying microrobots. IEEE Transactions on Power Electronics, 33(4), 3180–3191. https://doi.org/10.1109/TPEL.2017.2651038.

[3] Tuma, T., Sebastian, A., Lygeros, J., et al. (2013). The four pillars of nanopositioning for scanning probe microscopy: The position sensor, the scanning device, the feedback controller, and the reference trajectory. IEEE Control Systems Magazine, 33(6), 68–85. https://doi.org/10.1109/MCS.2013.2279620.

[4] Devasia, S., Eleftheriou, E., & Moheimani, S. O. R. (2007). A survey of control issues in nanopositioning. IEEE Transactions on Control Systems Technology, 15(5), 802–823. https://doi.org/10.1109/TCST.2007.902933.

[5] Gu, G. Y., Zhu, L. M., & Su, C. Y. (2014). Modeling and compensation of asymmetric hysteresis nonlinearity for piezoceramic actuators with a modified Prandtl-Ishlinskii model. IEEE Transactions on Industrial Electronics, 61(3), 1585–1595. https://doi.org/10.1109/TIE.2013.2261030.

[6] Kuhnen, K. (2003). Modeling, identification and compensation of complex hysteretic nonlinearities: A modified Prandtl-Ishlinskii approach. European Journal of Control, 9(4), 407–418. https://doi.org/10.3166/ejc.9.407-418.

[7] Stefanski, F., Minrowicz, B., Persson, J., et al. (2017). Non-linear control of a hydraulic piezo-valve using a generalized Prandtl-Ishlinskii hysteresis model. Mechanical Systems and Signal Processing, 83, 418–434. https://doi.org/10.1016/j.ymssp.2016.06.025.